Available online at www.sciencedirect.com
SCIENCE DIRECT
Journal of Catalysis 231 (2005) 181–193
JOURNAL OF CATALYSIS
www.elsevier.com/locate/jcat

The role of NO in the mechanism of NO_x reduction with ammonia over a BaNa–Y catalyst

Young Hoon Yeom [a], Juan Henao [a,b], Mei Jun Li [a], Wolfgang M.H. Sachtler [a,b], Eric Weitz [a,*]

[a] *Institute for Environmental Catalysis and Department of Chemistry, Northwestern University, Evanston, IL 60208, USA*
[b] *Center for Catalysis and Surface Science, Northwestern University, Evanston, IL 60208, USA*

Received 9 November 2004; revised 23 December 2004; accepted 12 January 2005

Abstract

NO reduces HNO_3 to HONO and surface nitrates to nitrites on a BaNa–Y zeolite, and it reacts with NO_2 to form N_2O_3. Data are also presented which show that adsorbed NO^+ reacts with water to form HONO. In the presence of NH_3 and H_2O these processes lead to the formation of ammonium nitrite, which efficiently decomposes near 100 °C to $N_2 + H_2O$, effecting the catalytic reduction of NO_x to N_2. A criterion for this path is that the optimum yield of N_2 is obtained with an equimolar mixture of $NO + NO_2$. Since ammonium nitrate, which can also form on this catalyst, does not significantly decompose at 200 °C, a typical temperature for diesel exhaust, the reduction of nitrate to nitrite serves to regenerate active sites on the BaNa–Y zeolite.

Keywords: NO_x reduction mechanism; Nitrate reduction on zeolites; Nitrate ions on zeolites; Ammonium nitrate; Ammonia; FT-IR; Nitrous acid

1. Introduction

Selective catalytic reduction (SCR) of nitrogen oxides (NO_x) with NH_3 is an efficient way to convert these toxic gases into environmentally benign N_2 [1–3]. Despite its importance, there is no clear consensus on the details of the mechanism of NO_x reduction with ammonia or other reductants, nor is there certainty about the commonality of the reaction paths over different catalysts. A possible clue with regard to the SCR mechanism is the effect of the NO/NO_2 ratio on the N_2 yield. There is generally negligible SCR for pure NO in the absence of O_2 and moderate SCR for NO_2, both in the presence and in the absence of O_2 at 200 °C, the typical temperature of diesel exhaust. Remarkably, however, much higher conversions of NO_x to N_2 have been reported for mixtures of NO and NO_2; the highest N_2 yield has been found for a 1:1 mixture of NO/NO_2. In 1981, Kato et al. reported that the SCR rate with ammonia was higher for an iron-titanium oxide catalyst when the reaction mixture contained an equimolar mixture of NO and NO_2 than for either only NO or only NO_2 [2]. Likewise, Tünter et al. reported that over a V_2O_5–WO_3–TiO_2 catalyst the highest SCR rate is achieved with a 1:1 NO/NO_2 mixture [3]. Koebel et al. found that the SCR performance over V_2O_5–WO_3/TiO_2 is highest with an equimolar mixture of NO and NO_2 [1]. More recently, Sun et al. [4] reported that NO_x is completely reduced by NH_3 over an Fe/MFI catalyst at low temperature. Isotopic labeling demonstrated that one N atom in each N_2 molecule is from NH_3 and the other is from NO.

Ramis et al. [5] suggest that nitrosamide, $NONH_2$, is an intermediate in NO_x reduction on NO_x catalysts working at high temperature. This model was also used by Topsøe et al. [6]. They assume that ammonia is oxidatively activated by V^5 to an N^{2-} species that reacts with NO. The nitrosamide is assumed to decompose to N_2 and H_2O. Koebel et al. later proposed that V^{4+} is reoxidized by NO_2 to V^{5+} in a process that yields nitrous acid as a co-product. Nitrous acid then reacts with adsorbed NH_3 to finally give $N_2 + H_2O$.

* Corresponding author.
E-mail address: weitz@northwestern.edu (E. Weitz).

0021-9517/$ – see front matter
doi:10.1016/j.jcat.2005.01.014

In the mechanism proposed by Sun et al. [4], HNO_2 is crucial; they propose that in the presence of NH_3 and H_2O the dynamic equilibrium

$$NO + NO_2 \leftrightarrow N_2O_3 \quad (1)$$

leads to the formation of ammonium nitrite, NH_4NO_2, by the reaction

$$N_2O_3 + 2NH_3 + H_2O \rightarrow 2NH_4NO_2. \quad (2)$$

Since 1847 it has been known that ammonium nitrite swiftly decomposes to N_2 and H_2O near 100 °C [7,8], leading to the overall reaction

$$NO + NO_2 + 2NH_3 \rightarrow 2N_2 + 3H_2O. \quad (3)$$

The reaction has a stoichiometry that is consistent with both the consumption ratio for NH_3, NO, and NO_2 and the fact that an optimum N_2 yield is obtained for an equimolar mixture of NO/NO_2.

IR spectroscopy has revealed that exposure of zeolite-based catalysts, such as Fe/MFI [9], Co/MFI [10], or Cu/MFI [10], to an atmosphere containing NO and O_2 results in the formation of nitro groups and nitrate ions. For BaNa–Y we recently reported that N_2O_4, the dimer of NO_2, is dissociatively chemisorbed to give NO^+ and NO_3^- ions [11]

$$N_2O_4 \rightleftharpoons (NO^+)_{ads} + (NO_3^-)_{ads}. \quad (4)$$

There is still a question as to whether these adsorbates react further or block sites of the catalyst. Whereas ammonium nitrite is known to easily decompose near 100 °C, the nitrate requires a much higher temperature, and its decomposition produces N_2O, a greenhouse gas. For low temperature applications, thermal decomposition would be expected to be insufficient to "protect" the catalyst against deactivation; chemical regeneration of the reactive surface site may be required.

The present study focuses on the reaction mechanism for NO_x reduction in the presence of NH_3 over a BaNa–Y zeolite. It is essential to clarify the role of NO in the reaction mechanism. NO will always coexist with NO_2 in the presence of oxygen as a result of the equilibrium $2NO + O_2 = 2NO_2$. A mechanism is proposed that rationalizes the particular efficiency of an equimolar NO/NO_2 mixture in NO_x reduction in the presence of excess ammonia. The data presented also indicate that *NO acts as a reductant for nitric acid, surface nitrates, and ammonium nitrate*. These critical and multiple roles for NO in a NO_x reduction mechanism do not seem to have been appreciated previously. This study also addresses the question of which steps in the reaction network are catalyzed, versus which can still occur efficiently in the absence of a catalyst.

2. Experimental

The zeolite samples were obtained by a threefold wet ion exchange of Na–Y (Si/Al = 2.5; Aldrich) with a 0.1 M $Ba(NO_3)_2$ solution at ambient temperature. For every exchange, the slurry was stirred for 48 h before it was vacuum filtered, washed thoroughly with doubly deionized H_2O, and dried in air. Elemental analysis via inductively coupled plasma spectroscopy (ICP) gave the following unit cell composition: $Ba_{9.6}Na_{33.8}Al_{53}Si_{139}O_{384}\cdot x H_2O$. Even though this zeolite acts functionally as a BaY zeolite [12], since there is a higher Na^+ than Ba^{2+} concentration, we refer to the sample as a BaNa–Y zeolite.

In situ FT-IR spectra were recorded in transmission mode with a Bio-Rad Excalibur FTS-3000 infrared spectrometer equipped with a MCT detector. Unless otherwise stated, we obtained each spectrum by averaging 70 scans at a resolution of 2 cm^{-1}. The "homemade" infrared cell, which is described in more detail in Ref. [11], is based on the design in Ref. [13] and consists of a stainless-steel cube with two CaF_2 windows that can be differentially pumped. The tungsten grid that supports the sample can be resistively heated to a temperature that is measured with a chromel–alumel thermocouple that is spot-welded to the center of the grid.

Typically, a small brush was used to "paint" 10–15 mg of zeolite, in a water slurry, onto a 1.5 × 1.5 cm tungsten grid while the grid was held at 353 K. The IR cell was then evacuated by a turbomolecular pump to a pressure of 5×10^{-7} Torr. The zeolite samples were heated under vacuum to 703 K and were kept at that temperature for 3–5 h to remove adsorbed water. A fresh zeolite sample was used for each set of new experiments. Samples of NO_2 were prepared by allowing a mixture of NO (typically 2 Torr) in a large excess of O_2 (typically 100 Torr) to reach equilibrium, so that the nitrogen-containing species in the mixture was virtually exclusively NO_2. These samples will be referred to as premixed samples or simply a "pre-mix." This procedure was used to produce NO_2 since it allowed for the production of isotopically labeled NO_2 from isotopically labeled NO without a change in the experimental protocol.

Catalytic tests were performed with a microflow reactor, which is described in more detail in Ref. [14]. NH_4NO_3/BaNa–Y (or quartz) samples used in these tests were prepared by the incipient wetness method, which involves impregnation of BaNa–Y (or quartz) (0.12 g) with an aqueous solution of 3.5 M NH_4NO_3 (0.12 g), followed by drying overnight at room temperature.

For experiments involving NH_4NO_3 and BaNa–Y or quartz, the feed gas was 20,000 ppm NO in helium which flowed through the reactor, held at 200 °C, at a flow rate of 10 standard cc/min. The reaction of HNO_3 with NO and NH_3 over BaNa–Y zeolite was studied at 200 °C in a system consisting of two microflow reactors arranged in series. Experiments were carried out for four different mixtures that flowed through the reactors at 100 ml/min. Helium was used to achieve the same overall flow rate in all reactor runs. The feed gases were as follows: (i) 1000 ppm HNO_3, which were introduced into the first reactor by bubbling He through a saturator containing a 55% HNO_3/water mixture; (ii) 1000 ppm HNO_3 and 1500 ppm NO, which resulted from a mixture of

NO in He being bubbled through a saturator containing the HNO_3/water mixture; (iii) 1000 ppm HNO_3 mixture was introduced into the first reactor and a mixture of 2000 ppm NH_3 in He was added to the flow in the second reactor; (iv) 1000 ppm HNO_3, 1500 ppm NO, and 2000 ppm NH_3, which resulted from the NO in He mixture being bubbled through the saturator containing the HNO_3/water mixture and NH_3 being added to the flow into the second reactor. Thus, in all cases the feed gas contained approximately 1% H_2O. In a typical experiment, the samples of BaNa–Y were loaded into the U-shaped quartz reactors, calcined in flowing O_2 at 500 °C for 2 h, and then cooled to 200 °C before being exposed to the reaction mixture. The mixtures leaving the saturator were directed through a reactor containing 200 mg of BaNa–Y at 200 °C. In experiments (iii and iv) in which both NH_3 and HNO_3 were present, ammonia was introduced into the system in the second reactor in the form of a mixture with He. This was done to minimize the interaction of HNO_3 and NH_3, since these compounds will rapidly react to form ammonium nitrate. Control experiments showed that this method of adding NH_3 minimizes NH_4NO_3 formation. As indicated in Section 3.4, under these conditions (iii and iv), a major portion of the original HNO_3 has already been reduced to HNO_2.

Dinitrogen formation was monitored on-line with a gas chromatograph with a thermal conductivity detector (TCD), with the use of an Alltech 5A molecular sieve column. To prevent condensation, heating tape was used to keep all lines at 80 °C. A NaOH solution (9 M) held at −10 °C was positioned before the GC to prevent acid vapors from entering the packed column. The N_2 yield was calculated from the amount of N_2 in the effluent and the amount of NO in the feed, except when only HNO_3 and NH_3 were used, in which case the amount of NH_3 in the feed was used. Nitric oxide (Matheson Tri-Gas, 98%), ^{15}NO (Cambridge Isotope, 98%), NO_2 (Matheson Tri-Gas, 99.5%), and NH_3 (BOC Gases, 99%) were used as received. Gaseous nitric acid was obtained from the vapor above a 1:2 (by volume) mixture of concentrated HNO_3 (69.6 wt% HNO_3; Fisher Chemical) and H_2SO_4 (95.7 wt%; Fisher Chemical).

3. Results

3.1. Adsorption of pre-mixes of $NO + O_2$

There are a number of IR studies of NO_x adsorbed by Na–Y [15] and Ba–Y [16] zeolites. In a previous investigation [11], we reported data on NO_2 adsorption on BaNa–Y at 200 °C. Details of the NO_2 adsorption mechanism are discussed in Ref. [11] and are not described here. However, some of the spectral changes that occur as a function of the BaNa–Y sample temperature are described, as they provide insights into the nature of the species present in these experiments.

Fig. 1 displays a series of IR spectra in the 1200–2300 and 3300–4000 cm^{-1} regions, recorded at different temperatures. When dehydrated BaNa–Y is exposed to 1.2 Torr of NO_2 at 33 °C, strong and broad absorption bands are immediately observed at 1352 and 1403 cm^{-1}. These are due to the symmetric and asymmetric vibrations of NO_3^- interacting with Ba^{2+} ions [11,15]. With increasing temperature the broad bands sharpen and separate into two more distinct bands at 1320 and 1438 cm^{-1} [15]. The feature centered at 1616 cm^{-1} is due to gas-phase NO_2. The intensity of this band increases slightly as the temperature is increased from 33 to 50 °C because of desorption of adsorbed $NO_3^- + NO^+$, which leads to an increase in the concentra-

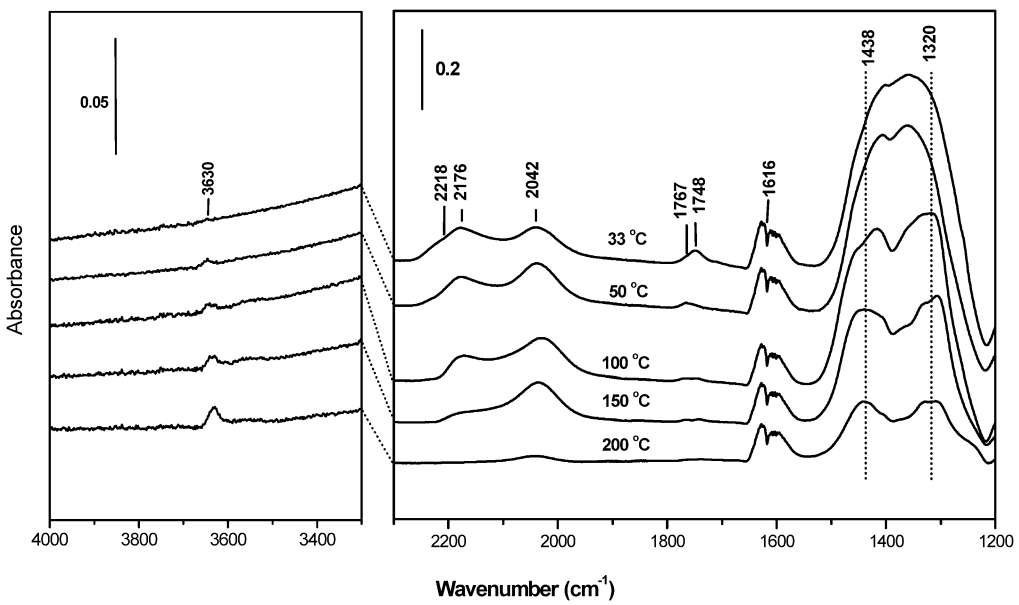

Fig. 1. FT-IR spectra observed upon exposing BaNa–Y to 61.2 Torr of the pre-mixture of 2 Torr of NO and 100 Torr of O_2 at 33 °C. After the exposure the temperature was gradually increased to 200 °C.

tion of gas-phase NO_2. However, increasing the temperature from 50 to 200 °C does not lead to a significant change in the intensity of the gas-phase NO_2 peak. This constant intensity is the result of two offsetting factors. One is simply desorption of adsorbed $NO_3^- + NO^+$, which increases with increasing temperature, and the other is the temperature dependence of the equilibrium, $2NO_2 \rightarrow 2NO + O_2$. Consistent with this explanation, the intensity of the gas-phase NO band (not visible on the absorbance scale shown) increases with increasing temperature. The center of the strongest peak in the gas-phase NO band is ∼ 0.00066 absorbance units (a.u.) at 33 °C and ∼ 0.0021 a.u. at 200 °C.

Increasing the temperature to 50 °C leads to a substantial diminishment in intensity of the band at 1748 cm^{-1}, whereas the absorption at 1767 cm^{-1} (shoulder) in Fig. 1 is still evident. Both of these bands gradually decrease in intensity with increasing temperature (from 50 to 150 °C) and are not visible in the trace taken at 200 °C (top trace). This region is where the asymmetric stretching modes of N_2O_4, along with the $\nu_1 + \nu_2$ combination vibration of NO_3^- ions, should absorb. Sedlmair [16] observed a band at 1763 cm^{-1}, at 50 °C, which they assigned to N_2O_4. In the present study, the absorption band at 1748 cm^{-1} is expected, at 33 °C, to contain a contribution from a N_2O_4 absorption. However, the relative importance of the contributions from these two species remains a point of controversy. The different temperature dependencies of these two bands (1748 and 1767 cm^{-1}) suggest that both N_2O_4 and NO_3^- contribute to these absorptions. Since higher temperature does not favor the formation of N_2O_4, the observed behavior is consistent with N_2O_4 contributing more significantly to the band at 1748 cm^{-1} at 33 °C.

Absorption bands at 2042, 2176, and 2218 cm^{-1} (shoulder) appear immediately after the exposure of BaNa–Y to NO_2 (see the spectrum in Fig. 1 taken at 33 °C). When the temperature is increased from 35 to 100 °C, the band at 2218 cm^{-1} completely disappears. The band at 2176 cm^{-1} gradually becomes weaker and is no longer visible at 200 °C, whereas the band at 2042 cm^{-1} increases in intensity as the temperature is increased from 33 to 50 °C, and thereafter there is no significant change in intensity up to 150 °C. However, there is a significant *decrease* in the intensity of this band when the temperature is increased from 150 to 200 °C. The band at 2218 cm^{-1} completely disappears with the evacuation of the cell (at 33 °C), as does the 2042 cm^{-1} band when the cell is evacuated at 200 °C. In previous work [11] we showed that the band at 2042 cm^{-1} is due to NO^+ that is formed by the reaction

$$N_2O_4 \rightarrow NO_3^- + NO^+. \quad (5)$$

Szanyi et al. used ^{15}NO and $^{18}O_2$ in a study of this process and assigned a band in the 2000–2200 cm^{-1} region to NO^+ [15]. The NO^+ interacts with the anionic zeolite framework oxygens. NO^+ can also interact with NO_2 to form $[NO^+ \cdot NO_2]$ and $[NO^+ \cdot N_2O_4]$ adducts, as suggested by Szanyi et al. [15] and Hadjiivanov et al. [17]. The IR absorptions of these adducts are in the 2100–2200 cm^{-1} region on Na–Y, and NO^+ is at 2020 cm^{-1} [17].

The stretching frequency of NO^+ depends on the degree of electron transfer of the corresponding anion to the π^* orbital of NO^+ [11]. Therefore, the stretching frequency of NO^+ varies with the nature and extent of exchange with the cation. The adducts alluded to above are relatively unstable, as indicated by the fact that they completely disappear at 200 °C. Combining our observations and literature results, we assign the two bands at 2176 and 2218 cm^{-1} to the $[NO^+ \cdot NO_2]$ and $[NO^+ \cdot N_2O_4]$ species adsorbed by anionic sites of framework oxygens.

As the temperature was increased from 33 to 200 °C, there was an ∼ 90% decrease in the integrated absorbance of the NO^+ species (at 200 °C), and the intensity of the NO_3^- absorption decreased by ∼ 75% at 200 °C. If these decreases were merely the result of desorption due to the back-reaction in Eq. (5), the percentage by which the intensity of these two bands decreased should be the same. As this is not the case, there must be another pathway for loss of NO^+, which is described below. The cause of the temperature-dependent change in intensity of the 3630 cm^{-1} band is also discussed below.

3.2. Reaction of $NO^+ + H_2O$

As discussed previously, when dehydrated BaNa–Y is exposed to NO_2 at 33 °C, absorption bands due to NO^+ and its adducts are seen at 2042, 2176, and 2218 cm^{-1}. As seen in Fig. 2, in which NO_2 interacts with BaNa–Y at 50 °C, bands at 2042 and 2176 cm^{-1} are visible, which are due to NO^+ and its adducts. As indicated above, the band at 2218 cm^{-1} decreases in intensity with temperature and is no longer visible at 50 °C. Surface nitrate at 1357 and 1413 cm^{-1}, gas-

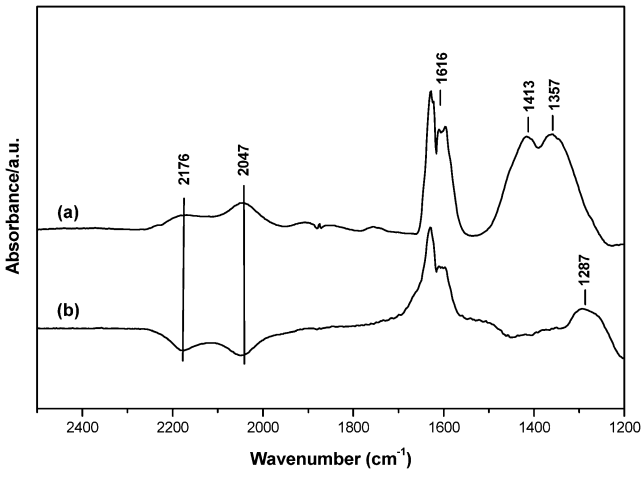

Fig. 2. (a) FT-IR spectra observed upon exposing BaNa–Y to 61.2 Torr of the pre-mixture of 2 Torr of NO and 100 Torr of O_2 at 50 °C. (b) After the same treatment as (a), the BaNa–Y is exposed to 104 Torr of pre-mix (100 Torr of He + 4 Torr of H_2O) at 50 °C. He in the pre-mix serves as a "carrier" for H_2O.

phase NO_2 at 1616 cm^{-1}, and gas-phase NO at 1876 cm^{-1} are also seen. Trace (b) in Fig. 2 is a difference spectrum obtained by subtraction of the spectrum taken after BaNa–Y has been exposed to NO_2 (trace a) from the spectrum taken after introduction of water to BaNa–Y zeolite that has been pre-exposed to NO_2. Effectively, we used trace (a) as the background spectrum in obtaining trace (b). After introduction of water, new bands are observed at 1287 (broad) and 1616 cm^{-1}. The increase in intensity of the band at 1616 cm^{-1}, which is due to gas-phase NO_2, is simply a result of compression of gas-phase NO_2 in the IR cell as a result of the introduction of water. On an extended time scale the NO_2 absorption gradually decreased as diffusion re-established a homogeneous distribution of the NO_2 and water in the cell. The assignment of the band at 1287 cm^{-1} will be discussed later.

The small negative bands at 1357 and 1413 cm^{-1} in trace (b) are due to displacement of NO_3^- by water on the zeolite surface. The two absorptions at 2047 and 2176 cm^{-1}, due to NO^+ and its adducts, disappeared with the introduction of water. The virtually instantaneous disappearance of these absorptions is clearly due to a reaction between water and NO^+ to give nitrous acid,

$$NO^+ + H_2O \rightarrow HNO_2 + H^+ \quad (6)$$

rather than simply the displacement of NO^+ from its adsorption site.

If the disappearance of NO^+ were caused by simple displacement by water, the intensity of the NO_3^- absorptions would decrease concomitantly, since NO_3^- is the counter-ion. Since there is almost no change in intensity of the NO_3^- absorptions during this process, it follows that the decrease in absorbance of the NO^+ must be due to a reaction with water, generating another counter-ion. If reaction (6) is operative, a positive band(s) in the O–H stretching region would be expected. However, under the conditions of the present experiment, such a band(s) could not be identified, presumably because of interference from the strong OH stretching vibration of water (not shown here) and/or interaction of water with the zeolite Brønsted acid sites. But, as seen in Fig. 1, an OH stretch band at 3630 cm^{-1} *was observed* when a low concentration of water was present in the cell. The most convenient way to achieve a suitably low concentration of water was to allow it to desorb from the cell walls. Furthermore, this band was not seen when dehydrated BaNa–Y was exposed to water. Thus, this band is due to a Brønsted acid site that is produced from the reaction between NO^+ and water (Eq. (6)). We attribute the slow increase in the intensity of this band at a fixed or increasing temperature to the reaction of NO^+ with water that is slowly desorbed from the IR cell walls. Consistent with this explanation, the 3630 cm^{-1} band due to the Brønsted acid sites gradually increased with exposure time at 200 °C. Further supporting this conclusion is the observation that the formation rate of this band is much slower when the cell has been pumped overnight with a turbopump while the sample was held at 703 K before being exposed to the pre-mix. Furthermore, it is known that NO^+ in the salts $NO^+HSO_4^-$, $NO^+ClO_4^-$, and $NO^+BF_4^-$ readily reacts with water to give $HNO_2 + H^+$ in a reaction analogous to that shown in Eq. (6) [18].

3.3. Assignment of the 1287 cm^{-1} band

Fig. 3 contains data relevant to the assignment of the 1287 cm^{-1} absorption. Trace (b) was obtained with the use of a mixture of $Ba(NO_2)_2$ and BaNa–Y. Trace (c) was obtained from a sample in which $Ba(NO_3)_2$ was mixed with BaNa–Y, and we obtained trace (d) by exposing BaNa–Y to NO_2. Two broad absorption bands, at 1264 and 1336 cm^{-1}, are observed in trace (b). Two very broad bands are also observed in traces (c) (at 1330 and 1435 cm^{-1}) and (d) (at 1353 and 1420 cm^{-1}). The absorption features in traces (c) and (d) would be expected to be similar, since both sets of bands are expected to be due to barium nitrate absorptions. Though the lower frequency band in trace (c) is at lower energy than the corresponding band in trace (d), both sets of bands (traces (c) and (d)) are shifted to higher energy compared with the bands in trace (b) (1264 and 1336 cm^{-1}) when $Ba(NO_2)_2$ is a component of the sample. The weak negative feature within the range 1310–1500 cm^{-1} in trace (a) is due to a loss of weakly bound surface nitrate. As mentioned in Section 3.2, this takes place with the introduction of water. As shown in reaction (6), water can react with NO^+ to form $HONO + H^+$. The H^+ then effectively acts as the counter-ion for the surface nitrate species, resulting in an equilibrium with HNO_3.

It is important to note that coordination of a nitrite anion to a metal cation can be accompanied by significant changes

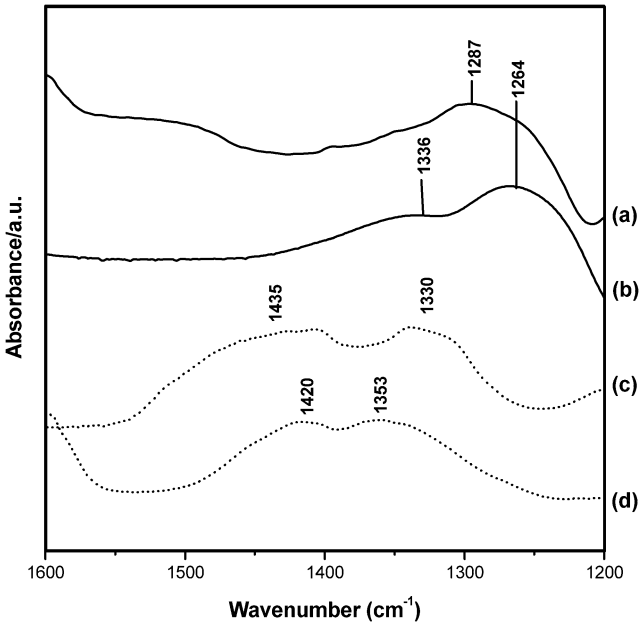

Fig. 3. (a) The same spectra as Fig. 2b, (b) spectra of $Ba(NO_2)_2$ that is diluted with BaNa–Y, (c) spectra of $Ba(NO_3)_2$ that is diluted with BaNa–Y, (d) spectra is obtained by exposing BaNa–Y to pre-mixture of $NO + O_2$.

in its IR spectrum. Therefore, there are considerable differences in the frequencies of IR bands that have been attributed to surface NO_2^-. For example, Szanyi et al. [15] reported that NO_3^- reacted with NO to give NO_2 and NO_2^-; they assign an absorption at 1275 cm^{-1} to NO_2^- species interacting with Na–Y. Sedlmair et al. [16] assigned absorptions at 1320 cm^{-1} for Na–Y and 1330 cm^{-1} for Ba–Y to the symmetric stretching vibration of surface nitrites, which are produced when the zeolite is exposed to NO_2. Prinetto et al. [19] observed an absorption at 1220 cm^{-1} upon exposing a Ba/Al_2O_3 surface to NO, which they assigned to a bidentate nitrite ion, the formation of which is ascribed to NO interacting with surface peroxide ions. The absorption frequencies of the chelating and the bridging bidentate nitrite species have been reported as 1266–1314 cm^{-1} ($\nu_{as}(NO_2)$) and 1176–1203 cm^{-1} ($\nu_s(NO_2)$), and the N=O stretch of monodentate nitrito and chelating nitro–nitrito species has been reported to be observed in the 1375–1470 and 1516–1435 cm^{-1} regions, respectively [20]. N–O stretching frequencies have been reported to be below 1210 cm^{-1} [20]. Nitro groups have been reported to have absorption frequencies in the 1375–1650 cm^{-1} region ($\nu_{as}(NO_2)$) and the 1250–1350 cm^{-1} region ($\nu_s(NO_2)$) [20].

It is unlikely that the absorption at 1287 cm^{-1} is due to a chelating nitro–nitrito group, since the frequencies for these species are typically at significantly higher energy [16]. It is also unlikely that this absorption is due to a nitro group, since it would require the less negatively charged N atom to interact with the cation. This frequency region is where an absorption of a chelating bidentate NO_2^- interacting with a barium cation would be expected, and we feel this is the most likely assignment. However, we cannot rule out the possibility that the 1287 cm^{-1} absorption corresponds to a species that is the same as or similar to the species observed by Szanyi et al. [12], which is shifted by ~ 12 cm^{-1} as a result of the difference in environment between the NaY and the BaNa–Y zeolites. This would imply that the only absorption in this region is due to a nitrite ion interacting with sodium cations. This would be surprising, since it would be expected that the interaction between a bidentate nitrite ion and Ba^{++} would be favored over the interaction of nitrite ions and Na^+ cations. However, we note that the specific nature of this species does not affect the discussion in the remainder of this paper.

3.4. Reduction of HNO_3 by NO

The spectra in Fig. 4a were obtained as a function of the indicated exposure time after introduction of gaseous HNO_3 into the reaction cell containing BaNa–Y held at 40 °C. This BaNa–Y sample had previously been dehydrated at 430 °C. Absorption bands at 1304 (strong and broad; not shown here), 1412 (strong and broad; not shown here), 1616, 1668, 1711, and 1767 cm^{-1} are observed in the top trace (20 s). As discussed, the bands at 1304 and 1412 cm^{-1} are due to surface nitrate [15,16]. The gas-phase absorption, centered

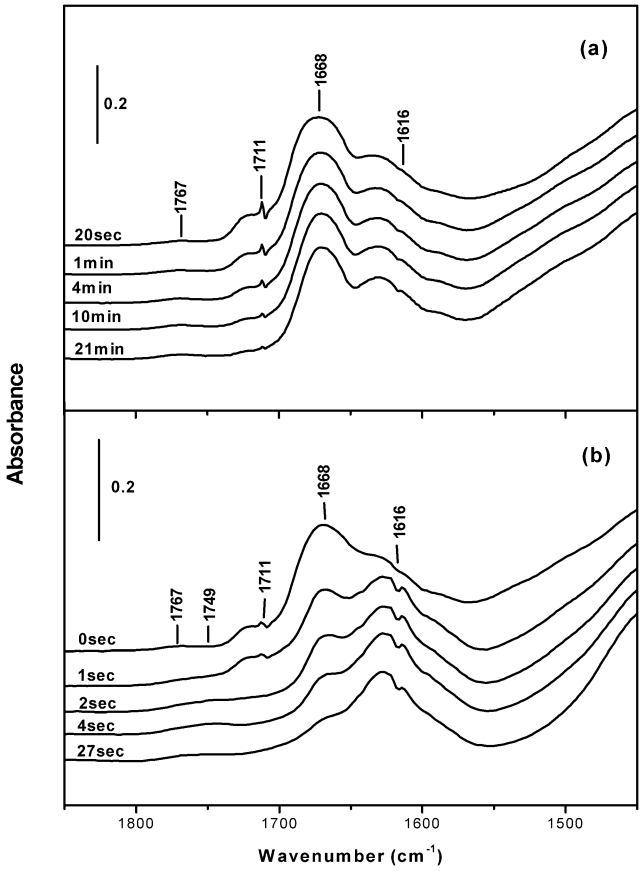

Fig. 4. (a) FT-IR spectra observed upon exposing BaNa–Y to 1.2 Torr of HNO_3 at 40 °C. The exposure time is indicated on each spectra, (b) FT-IR spectra observed upon exposing BaNa–Y, which is pre-exposed to 1.2 Torr of HNO_3, to 2.8 Torr NO.

at 1616 cm^{-1}, is due to NO_2 that results from the partial decomposition of HNO_3

$$2HNO_3 \rightarrow 2NO_2 + H_2O + \tfrac{1}{2}O_2. \quad (7)$$

The absorption centered at 1711 cm^{-1} is due to gas-phase HNO_3 [21], and, as discussed in Section 3.1, the absorption at 1767 cm^{-1} is due to a combination band of surface nitrate species [16]. This latter band is also seen when NO_2 is introduced into BaNa–Y.

The band at 1711 cm^{-1} gradually decreases in intensity as a function of exposure time. The broad and intense band at 1668 cm^{-1} becomes narrower and gradually decreases in intensity. Both of these changes are due to the slow adsorption of gas-phase HNO_3 on the BaNa–Y surface and the slow decomposition of HNO_3 via reaction (7). On porous glass and silica particles the corresponding band is observed to be somewhat higher in energy, at 1677 cm^{-1} [22].

The top trace in Fig. 4b was taken 4 min after the introduction of gaseous HNO_3 into BaNa–Y held at 40 °C. The feature is basically the same as in the top trace in Fig. 4a. The traces in the time-resolved spectra in Fig. 4b were taken after the introduction of NO into a sample of BaNa–Y that had been pre-exposed to HNO_3.

One second after the introduction of NO, ∼ 44% of the initially adsorbed HNO_3, as monitored at 1668 cm^{-1}, has disappeared (see second trace in Fig. 4b). In the absence of NO, even after 21 min of exposure, there is only an ∼ 26% decrease in the intensity of this band (see bottom trace of Fig. 4a). With added NO, after the rapid initial decrease in intensity, adsorbed HNO_3 undergoes a more gradual decrease as a function of exposure time. However, ∼ 28% of the adsorbed HNO_3 still remains after 27 s. These observations are consistent with the establishment of the following equilibrium

$$NO + HNO_3 \rightleftharpoons NO_2 + HONO. \quad (8)$$

In the presence of water there will also be an equilibrium involving both nitrogen oxides and HONO

$$NO + NO_2 + H_2O \rightleftharpoons 2HONO. \quad (9)$$

As expected from the thermodynamics of Eq. (9), which has a positive standard free energy for the formation of HONO [23], the concentration of HONO is small, and we did not directly detect adsorbed HNO_2 on the BaNa–Y surface from the above reaction. However, we did observe trace amounts of gaseous HNO_2 at 1264 cm^{-1}. In addition, HONO reacts with HNO_3 (10), and it can decompose on surfaces in a process that is the reverse of reaction (9)

$$HONO + HNO_3 \rightarrow 2NO_2 + H_2O. \quad (10)$$

By summing reactions (8) and (10), we can write a net reaction as follows

$$NO + 2HNO_3 \rightarrow 3NO_2 + H_2O. \quad (11)$$

This reaction has a small negative ΔG in the gas phase. Since NO does not strongly interact with Ba–NaY, it is possible that the ΔG is more negative on the surface because of the differential heat of adsorption of the species on the right side of the equation relative to those on the left side. The decrease in molecularly adsorbed HNO_3 is clearly due to a reaction with NO, since if the decrease were due simply to displacement by NO, there would be an increase in the intensity of gas-phase HNO_3, which absorbs at 1711 cm^{-1}. There is no such increase in gas-phase HNO_3, and, in fact, after the introduction of NO, gas-phase HNO_3 quickly disappears. As expected, the reaction of $NO + HNO_3$ has been observed to be even more rapid at a higher temperature (i.e., 70 °C; not shown).

To determine whether reaction (8) is catalyzed, the rates of consumption of HNO_3 in the presence and absence of BaNa–Y were compared. Dehydrated BaNa–Y was exposed to an equilibrium pressure of 1.7 Torr of HNO_3 at 40 °C, and subsequently 3.7 Torr of NO was introduced into the cell (see (b) in Fig. 5). With the introduction of NO, the band at 1711 cm^{-1}, due to gas-phase HNO_3, immediately disappeared, and absorptions due to NO_2 and HONO appeared at 1616 and 1264 cm^{-1}. The small amount of NO_2 that is present before the introduction of NO is a result of the slow decomposition of HNO_3 as shown in reaction (7) (see the second trace in Fig. 5b).

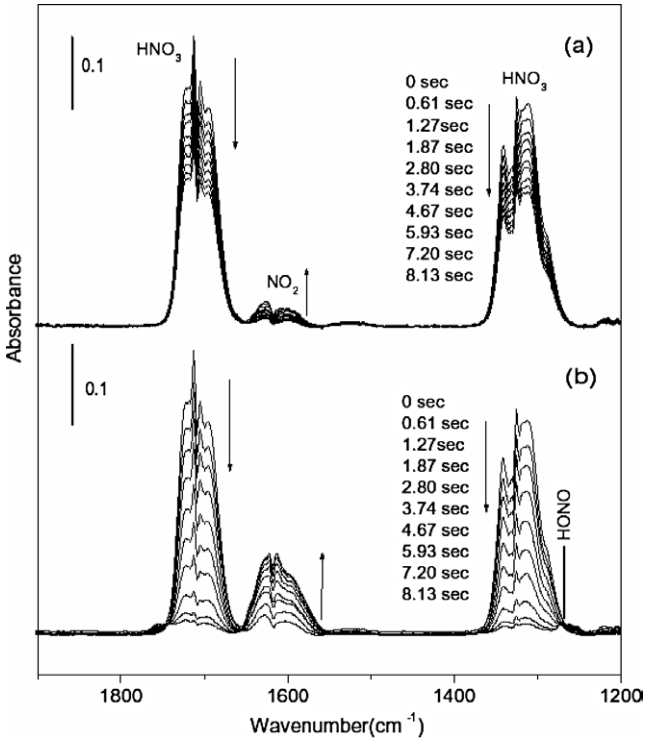

Fig. 5. (a) Time evolution of FT-IR spectra after 1.7 Torr of HNO_3 is introduced to an empty IR cell (tungsten mesh is present, but no zeolite) and 3.7 Torr of NO is subsequently introduced into the cell at 44 °C (grid temperature). Part (b) is the same as (a) but a BaNa–Y sample is present.

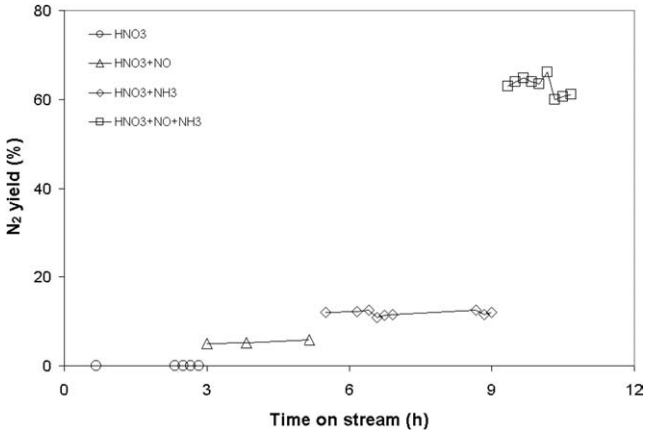

Fig. 6. The yield of N_2 on reaction of (i) HNO_3, (ii) $HNO_3 + NO$, (iii) $HNO_3 + NH_3$ and (iv) $HNO_3 + NO + NH_3$ over BaNa–Y at 200 °C in a flow reactor. Approximately 1% water was present in all the mixtures.

The reaction of $HNO_3 + NO$ was also run in the absence of BaNa–Y (Fig. 5a). These data clearly show that the reaction rate is significantly larger in the presence of BaNa–Y than in its absence. Thus, the BaNa–Y surface accelerates the reaction of $HNO_3 + NO$.

Fig. 6 contains data on the yield of N_2 from the reaction of flows of (i) HNO_3, (ii) $HNO_3 + NO$, (iii) $HNO_3 + NH_3$, and (iv) $HNO_3 + NO + NH_3$ over a BaNa–Y zeolite. As expected, HNO_3 alone does not yield significant N_2, and, based on GC data, there was no N_2 formation in experi-

ment (i). The mixture of NO and HNO_3 results in some nitrogen formation, although the ∼ 5% N_2 yield is still quite small. When NO is added to a flow of HNO_3, the color of the resulting mixture rapidly changes to brown. This is consistent with formation of NO_2, which is a co-product of the reduction of nitric acid to nitrous acid, as shown in Eq. (8). This observation implies that NO rapidly reduces nitric acid. With only NH_3 and HNO_3 in the feed gas (in the presence of ∼ 1% water) the main product is expected to be NH_4NO_3, and, consistent with this expectation, formation of a white powder is observed at the inlet of the second reactor. Since this powder is stable at 200 °C, its behavior is inconsistent with its being ammonium nitrite but consistent with the formation of ammonium nitrate. A priori, one could assume that in these experiments (iii) NH_3 might react with nitric acid via two pathways. It could act as a reductant, yielding nitrous acid, which would then react with ammonia to form ammonium nitrite, which is known to efficiently decompose at 200 °C, yielding N_2. An alternative reaction channel is the reaction of NH_3 with nitric acid to form ammonium nitrate, which is stable at the temperature of these experiments. The present results, showing a low nitrogen yield in experiment (iii), suggest that ammonia reacts preferentially with nitric acid to form ammonium nitrate. Quantification of these pathways and the relative efficiency of NO and NH_3 in reducing HNO_3 is currently the object of a study in our laboratory. Control experiments (not shown) indicate that, at the temperature of these experiments, once NH_4NO_3 begins to be deposited on the surface of BaNa–Y, nitrogen production decreases. However, when the feed contains HNO_3, NH_3, and NO (as in experiment (iv)), nitrogen production increases markedly.

In experiment (ii) the yield of N_2 is small and the path leading to its formation is not clear. Thus, we simply report the yield of nitrogen as the percentage of HNO_3 present, which is the reagent in lower concentration.

Experiment (iii) was conducted in the absence of added NO. In this case NH_3 must reduce HNO_3 to yield significant N_2. Such chemistry can be visualized as proceeding via the following reaction scheme:

$$3HNO_3 + 2NH_3 \rightarrow 3HONO + 3H_2O + N_2,$$
$$3HONO + 3NH_3 \rightarrow 3NH_4NO_2,$$
$$3NH_4NO_2 \rightarrow 3N_2 + 6H_2O \quad \text{which gives a net reaction of}$$

$$3HNO_3 + 5NH_3 \rightarrow 4N_2 + 9H_2O. \qquad (12)$$

As in experiment (iii), the limiting reagent is ammonia and the yield of N_2 is calculated as

$$\%N_2 = (\text{ppm } N_2 \text{ formed}) \times 1.25 \times 100/(\text{ppm } NH_3 \text{ in the feed}),$$

where the factor 1.25 comes from the relative stoichiometery for ammonia and N_2. Since ammonia is the limiting reagent, this yield represents a lower limit.

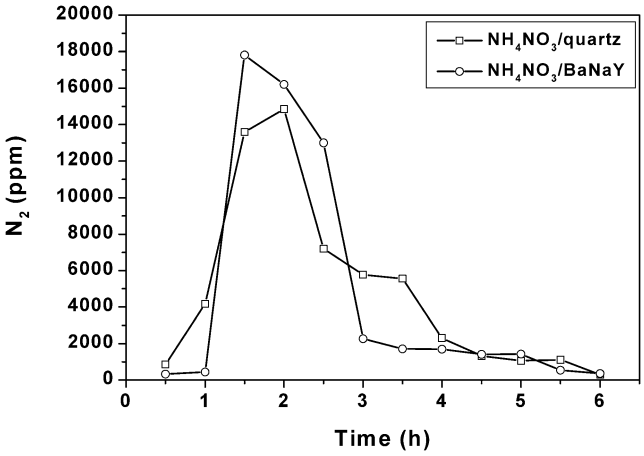

Fig. 7. The reaction of NO with NH_4NO_3 over BaNaY and quartz: NH_4NO_3 (0.12 g)/BaNaY (0.12 g), NH_4NO_3 (0.12 g)/quartz (0.12 g), NO: 20,000 ppm. The flow rate was 10 ml/min.

For experiment (iv), which is conducted in the presence of both NO and NH_3, the operative anticipated chemistry is

$$HNO_3 + NO \rightarrow HONO + NO_2,$$
$$NO + NO_2 + H_2O \rightarrow 2HONO,$$
$$3HONO + 3NH_3 \rightarrow 3NH_4NO_2,$$
$$3NH_4NO_2 \rightarrow 3N_2 + 6H_2O \quad \text{which gives a net reaction of}$$

$$HNO_3 + 2NO + 3NH_3 \rightarrow 3N_2 + 5H_2O. \qquad (13)$$

Here ammonia is the limiting reagent. Once it is depleted the formation of N_2 can still proceed, but now via the chemistry for reaction (ii), which has a much lower yield. Thus, the percentage yield of N_2 in experiment (iv) is calculated from the expression

$$(\text{ppm } N_2 \text{ formed}) \times 100/(\text{ppm } NH_3 \text{ in feed}),$$

where this yield is again a lower limit since ammonia is depleted before depletion of the other reactants.

Fig. 7 shows that when NO flows over quartz or BaNa–Y impregnated with NH_4NO_3, significant N_2 is produced. In fact, at the time of peak conversion (∼ 1.5 h after the flow is started) almost all of the NO is converted to N_2; there is a yield of ∼ 18,000 ppm of N_2 from 20,000 ppm of NO. The reaction sequence that is expected to lead to N_2 production is

$$NH_4NO_3 + NO \rightarrow NH_4NO_2 + NO_2, \qquad (14)$$

$$NH_4NO_2 \rightarrow N_2 + 2H_2O. \qquad (15)$$

3.5. The reaction between nitric oxide and surface nitrate

Dehydrated BaNa–Y held at 200 °C was exposed to 2 Torr of HNO_3 for 2 min. The cell containing the BaNa–Y sample was subsequently evacuated for 140 min, which was sufficient time to remove gas-phase HNO_3 and most of the HNO_3 that had adsorbed to the walls of the IR cell. However, as discussed below, even after 140 min of evacuation time some HNO_3 still remained adsorbed. The resulting

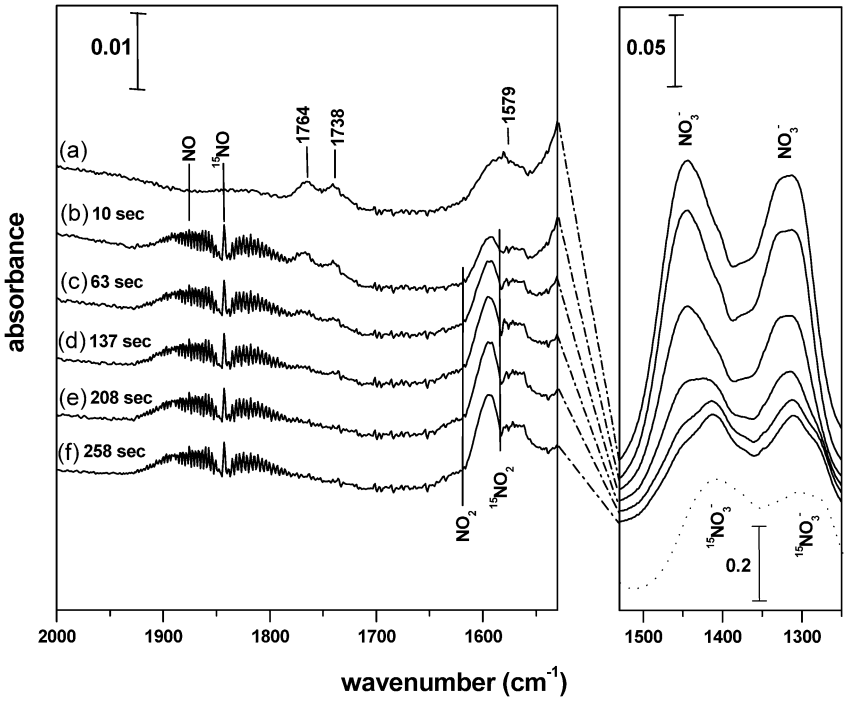

Fig. 8. (a) FT-IR spectra recorded after 140 min of evacuation of the cell containing a BaNa–Y sample that had been exposed to 2 Torr of HNO_3 at 200 °C. Traces (b)–(f) after introduction of NO, with the exposure time shown for each spectrum.

spectrum is shown in Fig. 8a. After evacuation of the IR cell, 1.4 Torr of ^{15}NO was subsequently introduced into the cell. The series of spectra, (b)–(f) shown in Fig. 8, were taken as a function of the indicated exposure time following the introduction of ^{15}NO. We obtained the dashed trace on the right side of the figure by exposing dehydrated BaNa–Y to 1.2 Torr of $^{15}NO_2$ at 200 °C. The dashed trace shows only ^{15}N-surface nitrate species in the given region.

Strong and broad absorption bands at 1315 and 1443 cm^{-1} that are due to surface nitrate are seen in trace (a). The surface nitrate that is initially formed after the introduction of 2 Torr HNO_3 is ∼ 60% removed by evacuation for 210 min at 200 °C. Additional evacuation for 30 min results in only a small change in the intensity of these bands. The absorption at 1579 cm^{-1} is probably due to NO_3^- that interacts with extraframework alumina. Interestingly, this band is seen when the zeolite is exposed to HNO_3, but the band is weak or not observable after the introduction of NO_2. Sedlmair et al. [16] attributed a feature at 1580 cm^{-1}, which was formed on Ba–Y after the introduction of NO_2, to chelating nitrate, which interacts with extraframework alumina. The bands at 1764 and 1738 cm^{-1} are due to the combination bands of surface nitrate described in Section 3.1. The intensities of these bands *decrease* with NO exposure time.

After the introduction of ^{15}NO, the intensity of the surface nitrate bands decreases and gas-phase features of $^{15}NO_2$, NO_2, ^{15}NO, and NO are observed at 1581, 1616, 1842, and 1875 cm^{-1}, respectively (see trace (b)). The intensity of the surface nitrate absorptions rapidly decrease for the first minute after ^{15}NO exposure; however, after 208 s there is only a slow change in intensity. Beyond 258 s, at which point the intensity of the surface nitrate has decreased by ∼ 66%, there is no significant further change in intensity.

Subsequent to exposure to ^{15}NO, the position of the surface nitrate absorption shifts to lower wavenumbers. The spectrum after 208 s of exposure to ^{15}NO is shown in trace (e), and the nitrate absorption shifts even further to lower frequency ∼ 258 s subsequent to the addition of ^{15}NO. After 258 s of exposure the peaks at 1315 and 1443 cm^{-1} have shifted to 1291 and 1409 cm^{-1}, respectively (compare traces (a) and (f)). Beyond 258 s of exposure, there is little change in either the shape or the position of the surface nitrate absorptions.

The positions of absorptions of the surface nitrate species in trace (f) match well with the surface $^{15}NO_3^-$ species in the dashed trace in Fig. 8. Hence, it is clear that ^{15}N replaces ^{14}N on the surface

$$^{15}NO + NO_3^- \rightarrow NO + {}^{15}NO_3^-. \quad (16)$$

The decrease in intensity of the surface nitrate absorption is probably due to the following surface reactions

$$^{15}NO + (H^+)_{ad} + (NO_3^-)_{ad} \rightarrow {}^{15}NO_2 + HNO_2, \quad (17)$$

$$(HNO_3)_{ad} + HNO_2 \rightarrow 2NO_2 + H_2O. \quad (18)$$

The intensity of the gas-phase NO_2 absorption is always smaller than the intensity of the $^{15}NO_2$ absorption, since there is an equilibrium between the NO_2 produced in the above reaction and excess ^{15}NO

$$NO_2 + {}^{15}NO \rightarrow NO + {}^{15}NO_2. \quad (19)$$

Despres et al. [24] have studied the influence of NO on the adsorption and desorption of NO_2 on BaO/TiO_2. They

showed that chemisorption of NO_2 in this system is dissociative, with concomitant release of NO into the gas phase

$$3NO_2 + BaO \rightarrow NO + Ba(NO_3)_2. \quad (20)$$

If NO is added to the feed, the previously formed nitrate begins to react to form NO_2 at $\sim 200\,^{\circ}C$. Based on this observation, they proposed that NO reacts with the previously formed NO_3^-, yielding NO_2 as an intermediate

$$NO + Ba(NO_3)_2 \rightarrow 3NO_2 + BaO. \quad (21)$$

Immediately after the introduction of ^{15}NO (see trace (C) in Fig. 8) we observe both $^{15}NO_2$ and a decrease in the intensity of surface ^{14}N-nitrate. This indicates that reaction (17) is rapid. As a control, the same experiment was conducted without a zeolite sample. $^{15}NO_2$ also appeared rapidly in the gas phase with the introduction of ^{15}NO into a cell that had been exposed to nitric acid. This $^{15}NO_2$ is the result of similar reactions described in Section 3.4

$$^{15}NO + HNO_3 \rightarrow {}^{15}NO_2 + HNO_2. \quad (22)$$

Since HNO_3 was strongly adsorbed to the walls of the cell, its removal was incomplete even after 140 min of evacuation time. The fact that the temperature of the IR cell *wall was not* 200 °C, but was closer to room temperature, contributes to the ability of HNO_3 to remain adsorbed. Since there could be multiple sources of $^{15}NO_2$ (reaction on the zeolite and reaction in the gas phase and/or on the walls of the IR cell), the concentrations of $^{15}NO_2$ and NO_2 were quantified for these situations. Only $\sim 20\%$ of the total amount of $^{15}NO_2 + NO_2$ in traces (b)–(f) is due to reactions of nitric acid from or on the IR cell wall, and the remaining 80% is due to reactions on the zeolite sample. Based on literature data [23], reaction (22) is slightly endothermic in the gas phase at 473 K (~ 9 kJ/mol) but could easily be thermodynamically favored on BaNa–Y because of the free energy of adsorption of the species on the right side of Eq. (22) is greater than that on the left side. Since NO only weakly interacts with the surface, this appears to be plausible.

Though a surface nitrite is predicted by reaction (17), we have not been able to directly observe this surface nitrite under these conditions. This is probably due to its small steady-state concentration as a result of its expected efficient thermal decomposition at 200 °C. Moreover, as previously discussed, the expected nitrite absorption band overlaps with a strong surface nitrate band. Stark et al. [25] studied isotopic labeling of soil nitrate with the use of ^{15}N-nitric oxide gas under dry conditions at room temperature. They found that NO_3^- was 90% labeled by ^{15}N after 2 h of contact time. They also found that almost all of the initially observed $^{14}NO_2^-$ was converted to $^{15}NO_3^-$ by 20 h after exposure to ^{15}NO.

Beutel et al. studied nitrogen isotope exchange between gaseous NO_y and chemisorbed NO_y groups on Cu-ZSM-5, where NO_y denotes all adsorption complexes that are obtained with exposure of catalysts to a mixture of $NO + O_2$ [10a]. They proposed that the monodentate nitrate is more active than the bidentate species and that the $^{15}NO_2$ moiety of the monodentate nitrate, Cu–O–$^{15}NO_2$, undergoes exchange with physisorbed ^{14}NO at room temperature. The exchange results in the formation of Cu with ligating ^{14}N-nitrite and physisorbed $^{15}NO_2$ [10a]. Jordan et al. [26] studied the exchange of nitrogen between nitric oxide and aqueous solutions of nitric acid with the use of ^{15}NO. They showed that nitrogen exchange was limited by NO_3^-–HNO_2 exchange, where the HNO_2 was formed by oxidation of NO by HNO_3. Though we are not in a position to discuss the mechanistic details of reaction (16), this reaction probably takes place via an $^{15}NO_2$ intermediate

$$^{15}NO_2 + NO_3^- \rightarrow {}^{15}NO_3^- + NO_2. \quad (23)$$

This hypothesis is supported by the fact that reactions (17) and (18) appear to be faster than reaction (23), as judged by the following observations. ^{14}N-surface nitrate first decreased and the band position gradually shifted to the lower wavenumbers of ^{15}N-surface nitrate. Second, if $^{15}NO_2$ is introduced instead of ^{15}NO under the same conditions, nitrogen exchange between $^{15}NO_2$ and NO_3^- is relatively faster than that observed when NO is added.

4. Discussion

4.1. Nitrous acid formation

As seen in Fig. 1, when BaNa–Y is exposed to NO_2, formation of NO^+ and NO_3^- is effectively immediate. N_2O_4, which is in equilibrium with gas-phase NO_2 (Eq. (5)), dissociatively adsorbs by the BaNa–Y zeolite to give NO^+ and NO_3^-. Once formed on BaNa–Y, NO^+ is quite stable *in the absence* of water; it is readily observable even at 200 °C. However, it reacts very rapidly with water to form nitrous acid. As discussed in Section 3.3, the band at 1287 cm^{-1} is a spectroscopic marker for surface nitrite species. As seen in Fig. 2, subsequent to the formation of NO^+ and the addition of water to the reaction cell, surface nitrite is observed for a BaNa–Y sample held at 50 °C. In this environment the formation of H^+ is expected, since the loss of NO^+ relative to NO_3^- requires the formation of a new counter-ion, and the absorption at 3630 cm^{-1}, seen in Fig. 1, is characteristic of H^+. In fact, H^+, surface NO_2^-, and HONO are expected to be in equilibrium as a result of reaction (24)

$$HONO \leftrightarrow H^+ + NO_2^-. \quad (24)$$

However, as alluded to above, a high steady-state concentration of HONO is not expected, since it is very reactive and dissociates easily, and, as discussed in Section 3.4, depending on conditions, it can be a participant in other competitive equilibria.

4.2. The role of NO_3^-

As indicated above, when NO^+ is produced by dissociative adsorption of N_2O_4, NO_3^- is the co-product. We now consider the fate of this species.

We observed that both gas-phase HNO_3 and surface nitrate are formed by exposure of hydrated BaNa–Y to NO_2. Spectroscopic markers due to H^+ are also present. Nitric acid can react with NH_3 to form ammonium nitrate [27]. This is a more thermally stable species than ammonium nitrite. Data in Ref. [28] show that ammonium nitrate does not appreciably dissociate until its temperature reaches $\sim 312\,^\circ C$ and that the primary dissociation product is N_2O. Thus, for efficient low-temperature reduction of NO_x to N_2, *formation of ammonium nitrate is undesirable, whereas formation of ammonium nitrite is desirable*. As discussed below, NO is an important species in the NO_x reduction process, since it acts as a reductant for both nitric acid and surface nitrate.

4.3. The role of NO in NO_x reduction

The data in Fig. 4 relate to another important reaction of nitric acid that can take place in a NO_x environment. Adsorbed HNO_3 reacts with NO to form HONO. This is clearly seen in Fig. 5b, in which the gas phase over a BaNa–Y sample is probed. After the BaNa–Y sample is exposed to nitric acid, NO is introduced into the IR cell. The HNO_3 rapidly disappears, NO_2 is formed, and, along with the NO_2, gas-phase HONO is seen at 1264 cm^{-1}. As demonstrated by the data in Fig. 5a, reaction (8) can take place in the gas phase in the absence of BaNa–Y. However, a comparison of the data in Figs. 5a and b shows clearly that reaction (8) *is accelerated* in the presence of BaNa–Y. In the presence of BaNa–Y, approximately half of the HNO_3 has reacted in 2.8 s, whereas in the absence of BaNa–Y half of the HNO_3 is still present after 8 s. To demonstrate that adsorbed HNO_3 reacts with NO on BaNa–Y, a BaNa–Y sample that had been pre-exposed to HNO_3 was subsequently exposed to NO (see Fig. 4b). On exposure to NO the intensity of a peak due to adsorbed HNO_3, at 1668 cm^{-1}, rapidly decreases and NO_2 is produced. In the absence of NO, the adsorbed HNO_3 is stable. The production of NO_2 strongly suggests that HONO is a co-product of this reaction, which is catalyzed by BaNa–Y, and thus that HNO_3 is reduced to HNO_2 by NO.

In either case, once HONO is formed, NO_x reduction can take place via the route discussed in Section 3.4. The relevant steps in this mechanism are summarized in Scheme 1. One conclusion from the mechanism shown in Scheme 1 is that in the absence of added NO, ammonium nitrate will form. Since ammonium nitrate is relatively stable compared with ammonium nitrite, and its main decomposition product is N_2O, its formation can reduce the yield of N_2 in a deNO_x process. *The presence of NO leads to competitive reaction pathways that reduce the formation of ammonium nitrate and enhance the yield of nitrous acid*. As shown in Scheme 1, nitrous acid will then react with ammonia to form ammonium nitrite. NO can also chemically reduce ammonium nitrate to ammonium nitrite. Consistent with this picture, data in Fig. 6 show that the addition of NO *increases* the yield of N_2 from a HNO_3 stream in the presence of excess NH_3.

Consistent with this observation, in a prior work [28] we observed that the N_2 yield increased when NO was added to a stream of $NO_2 + NH_3 + O_2$ flowing over a BaNa–Y zeolite. Effectively, each molecule of NO reacts with a molecule of HNO_3 to form a molecule of nitrous acid *instead of a molecule of ammonium nitrate*. As stated above, and as seen in Scheme 1, the formation of nitrous acid allows the system to continue on the pathway for NO_x reduction, whereas formation of ammonium nitrate effectively "traps" a NO_x molecule in the form of a less reactive species. If the reaction pathway for the formation of NH_4NO_3 in Scheme 1 is completely suppressed, the net reaction can be then expressed as

$$NO_2 + NO + 2NH_3 \rightarrow 2N_2 + 3H_2O. \quad (25)$$

Reaction (25) then requires an equimolar mixture of NO and NO_2 for optimum N_2 production.

We also note that, as seen in Fig. 6, NO by itself is relatively inefficient at reducing ammonia at 200 °C over BaNa–Y. The mechanism in Scheme 1 is consistent with this observation, since there is no direct pathway for NO_x reduction involving only NO. NO_2 is required to initiate the process, which in this system occurs via dimerization and dissociative adsorption of N_2O_4 to give NO^+ and NO_3^-.

As discussed in Section 3.5, NO acts as a reductant of surface nitrate ions. The data in Fig. 7 directly demonstrate that NO can also act as a reductant for NH_4NO_3. The introduction of NO to either quartz or BaNa–Y that is impregnated with NH_4NO_3 leads to a significant yield of N_2, which does not occur in the absence of added NO. This result is consistent with a reduction process similar to that illustrated in Eqs. (14) and (15), taking place with ammonium nitrate, yielding ammonium nitrite, which can be readily decomposed at the temperature of these experiments to yield N_2.

This is a very significant result. Formation of ammonium nitrate can decrease the activity of the BaNa–Y catalyst toward NO_x reduction in the presence of ammonia. NO can also be viewed as effectively "cleaning" the zeolite surface. Since surface nitrates are stable at 200 °C, a chemical means is needed to remove these species and activate the sites occupied by the nitrates for further chemistry—presumably chemistry involving nitrites. As discussed in Section 3.5, NO can perform this function by reducing surface nitrates to nitrites. Thus, there are multiple processes that involve NO that either inhibit ammonium nitrate formation or facilitate its conversion and/or the conversion of precursors to this species to readily decomposable ammonium nitrite. This multifaceted role for NO in the SCR of NO_x with

ammonia does not seem to have been recognized previously.

4.4. The role of ammonium nitrite in NO_x reduction processes over other catalysts

The pathways for the formation of ammonium nitrite and its decomposition to $N_2 + 2H_2O$, which are shown in Scheme 1, have low activation energies, even in the absence of a catalyst. Thus, the reaction pathway for the production of N_2 and H_2O, via NH_4NO_2, is likely to be operative for other catalysts that are active for the SCR process with ammonia. Indeed, Long et al. [29] report that over an Fe–Mn-based oxide catalyst, the reduction of NO with NH_3 to N_2 is likely to proceed via ammonium nitrite. For SCR over a vanadia–titania catalyst Madia et al. [1] report that the reaction is much faster with a feed with a 1:1 NO/NO_2 ratio than with pure NO_2. In comparison with a feed gas containing $NO + O_2$ in a 4:1 ratio, the reduction with ammonia of the $NO/NO_2 = 1{:}1$ feed, below 250 °C, was 10 times faster. This indicates that even over this transition metal catalyst, the oxidation of 50% of the NO to NO_2 is slower than the formation of N_2 from NH_3 and the $NO/NO_2 = 1{:}1$ mixture.

If this is the basic chemistry for catalytic reduction of NO_x, it follows that the catalyst has two main tasks:

1. Convert the inlet NO_x to a mixture with a NO/NO_2 ratio equal to or approaching 1:1;
2. If the primary reductant is not ammonia but a hydrocarbon or another organic molecule, then the catalyst must convert part of the NO_x feed to NH_3.

Thus, the ideal catalyst should convert a feed containing NO_x, O_2, and any reductant to a mixture of NH_3, NO, and NO_2 in a ratio of 2:1:1.

5. Conclusions

NO plays a critical role in the NO_x reduction process in the presence of ammonia. NO reacts with a number of species that are present during NO_x reduction with ammonia to open up competitive reaction pathways that lead to ammonium nitrite, which then decomposes to N_2 and water at temperatures greater than or approximately equal to 100 °C. The present studies demonstrate that NO can reduce nitric acid, surface nitrates, and ammonium nitrate.

As seen in Scheme 1, in the absence of added NO, nitric acid reacts with ammonia to form ammonium nitrate, which is thermally stable at the ∼ 200 °C temperature of these experiments (and of diesel exhaust). The formation of ammonium nitrate reduces the activity of the BaNa–Y zeolite for NO_x reduction in the presence of ammonia. How-

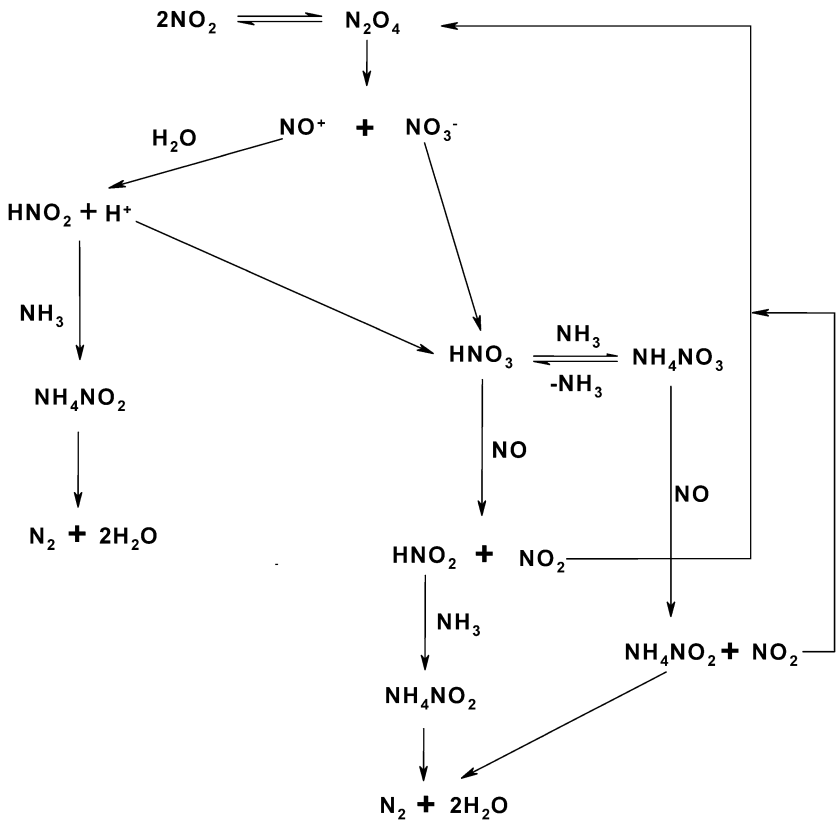

Scheme 1.

ever, NO reduces nitric acid to nitrous acid. Nitrous acid can then react with NH_3 to form ammonium nitrite, which readily decomposes at $\sim 100\,^{\circ}C$. In addition, reduction of surface nitrates to nitrites by NO provides another pathway for the production of nitrous acid that can subsequently react to form ammonium nitrite. We also present data which show that NO can act as a reductant for ammonium nitrate. NO can also react with NO_2 to form N_2O_3, which can then react with ammonia and water to form ammonium nitrite.

Thus, NO participates in a number of reactions in the NO_x reduction network. These reactions serve as pathways to nitrous acid and eventually, either directly or indirectly, to ammonium nitrite, which thermally decomposes, at a temperature greater than or approximately equal to $100\,^{\circ}C$, to water and N_2, the desired products for SCR of NO_x. Reaction (25) rationalizes the observation that the optimum yield of N_2 is obtained with an equimolar mixture of NO/NO_2 in the presence of excess ammonia. In fact, as we have demonstrated in a prior work [28], when there is an excess of NO_2 relative to NO, the introduction of an incremental additional amount of NO increases the yield of N_2 on a molecule-for-molecule basis.

The mechanistic conclusions of this work are summarized in Scheme 1.

Acknowledgments

This work was supported by the EMSI program of the National Science Foundation and the U.S. Department of Energy, Office of Science (CHE-9810378) and by Chemical Sciences, Geosciences and Biosciences Division, Office of Basic Energy Sciences, Office of Science, U.S. Department of Energy, Grant No. DE-FG02-03ER15457 at the Northwestern University Istitute for Environmental Catalysis.

References

[1] M. Koebel, M. Elsener, G. Madia, Ind. Chem. Eng. Res. 40 (2001) 52.
[2] A. Kato, S. Matsuda, T. Kamo, F. Nakajima, H. Kuroda, T. Narita, J. Phys. Chem. 85 (1981) 4099.
[3] G. Tuenter, W. Leeuwen, L. Snepvangers, Ind. Eng. Chem. Prod. Res. Dev. 25 (1986) 633.
[4] Q. Sun, Z.-X. Gao, H.-Y. Chen, W.M.H. Sachtler, J. Catal. 201 (2001) 89.
[5] G. Ramis, G. Busca, F. Bregani, P. Forzatti, Appl. Catal. B 64 (1990) 259.
[6] N.Y. Topsøe, Science 265 (1994) 1217.
[7] E. Millon, Ann. Chim. Phys. 3 (19) (1847) 255.
[8] F. Notoya, C. Su, E. Sasaoka, S. Nojima, Ind. Eng. Chem. Res. 40 (2001) 3732.
[9] (a) H.Y. Chen, T.V. Voskoboinikov, W.M.H. Sachtler, J. Catal. 180 (1998) 171;
(b) H.Y. Chen, T.V. Voskoboinikov, W.M.H. Sachtler, J. Catal. 186 (1999) 91.
[10] (a) T. Beutel, B.J. Adelman, W.M.H. Sachtler, Appl. Catal. B Environ. 9 (1996) L1;
(b) B.J. Adelman, T. Beutel, G.-D. Lei, W.M.H. Sachtler, J. Catal. 158 (1996) 327.
[11] Y.H. Yeom, B. Wen, W.M.H. Sachtler, E. Weitz, J. Phys. Chem. B 108 (2004) 5386.
[12] G. Panov, R.G. Tonkyn, M.L. Balmer, C.H.F. Peden, Soc. Automot. Eng. (2001) 01–3513.
[13] P. Basu, T.H. Ballinger, J.T. Yates, Rev. Sci. Instrum. 59 (1988) 1321.
[14] (a) B. Wen, Q. Sun, W.M.H. Sachtler, J. Catal. 204 (2001) 314;
(b) B. Wen, W.M.H. Sachtler, Catal. Letter 86 (2003) 39.
[15] J. Szanyi, J.H. Kwak, R.A. Molina, C.H.F. Peden, Phys. Chem. Chem. Phys. 5 (2003) 4045.
[16] C. Sedlmair, B. Gil, K. Seshan, A. Jentys, J.A. Lercher, Phys. Chem. Chem. Phys. 5 (2003) 1897.
[17] K.I. Hadjiivanov, B. Tsyntsarski, T. Nikolova, Phys. Chem. Chem. Phys. 1 (1999) 4521.
[18] F.A. Cotton, G. Wilkinson, in: Advanced Inorganic Chemistry, fifth ed., Wiley, New York, 1988, pp. 322–323.
[19] F. Prinetto, G. Chiotti, I. Nova, L. Castoldi, L. Lietti, E. Tronconi, P. Forzatti, Phys. Chem. Chem. Phys. 5 (2003) 4428.
[20] K.I. Hadjiivanov, Catal. Rev. Sci. Eng. 42 (2000) 71.
[21] M. Mochida, B.J. Finlayson-Pitts, J. Phys. Chem. A 104 (2000) 8038.
[22] A.L. Goodman, G.M. Underwood, V.H. Grassian, J. Phys. Chem. A 103 (1999) 7217.
[23] NIST Webbook, http://webbook.nist.gov/, Standard state entropies and enthalpies were used for calculation of ΔG at $40\,^{\circ}C$.
[24] J. Despres, M. Koebel, O. Krocher, M. Elsener, A. Wokaun, Appl. Catal. B, Environ. 43 (2003) 389.
[25] J.M. Stark, M.K. Firestone, Soil. Sci. Soc. Am. J. 59 (1995) 844.
[26] S. Jordan, F.T. Bonner, Inorg. Chem. 12 (1973) 1369.
[27] See Ref. [18], p. 315
[28] M. Li, Y.H. Yeom, E. Weitz, W.M.H. Sachtler, Catal. Lett. 98 (2004) 5.
[29] R.Q. Long, R.T. Yang, R. Chang, Chem. Commun. (2002) 452.